Asian Journal of Atmospheric Environment
Vol. 9-1, pp. 22-30, March 2015
doi: http://dx.doi.org/10.5572/ajae.2015.9.1.022

ISSN(Online) 2287-1160
ISSN(Print) 1976-6912

A CFD Study of Roadside Barrier Impact on the Dispersion of Road Air Pollution

Sang Jin Jeong*

Department of Energy and Environmental Engineering, Kyonggi University, Suwon, Gyeonggi-do 442-760, Korea

*Corresponding author. Tel: +82-31-249-9734, E-mail: sjjung@kyonggi.ac.kr

ABSTRACT

This study evaluated road shape and roadside barrier impact on near-road air pollution dispersion using FLUENT computational fluid dynamics (CFD) model. Simulated road shapes are three types, namely at-grade, depressed, and filled road. The realizable $k-\varepsilon$ model in FLUENT CFD code was used to simulate the flow and dispersion around road. The selected concentration profile results were compared with the wind tunnel experiments. The overall concentration profile results show good agreement with the wind tunnel results. The results showed that noise barriers, which positioned around the at-grade road, decrease the horizontal impact distance (In this study, the impact distance was defined as the distance from road surface origin coordinate to the position whose mass fraction is 0.1.) lower 0.33~0.65 times and change the vertical air pollution impact distance larger 2.0~2.27 times than those of no barrier case. In case of filled road, noise barriers decrease the horizontal impact distance lower 0.24~0.65 times and change the vertical air pollution impact distance larger 3.33~3.55 times than those of no barrier case. The depressed road increase 1.53~1.68 times the vertical air pollution impact distance. It contributes the decrease of horizontal air pollution impact distance 0.32~0.60 times compare with no barrier case.

Key words: CFD model, Road shape, Noise barrier, Road emission, Air pollution dispersion

1. INTRODUCTION

Roadside noise barriers are common features along major highways in urban regions and are anticipated to have important effects on near-road air pollution through altering the dispersion of traffic emissions and resulting downstream concentrations (Hagler *et al.*, 2011). Studies have shown that people who live near roadways are at risk for a variety of health problems, including respiratory and cardiovascular problems, birth and developmental defects, and cancer, due to exposure to harmful traffic-related air pollutants (HEI, 2010). Vehicle-related toxic emissions from roadways include such pollutants as particulate matter, carbon monoxide, heavy metals, and volatile organic compounds.

There is a growing need for developing mitigation strategies for near-road air pollution. Roadway design is being considered as one of the potential options. Particularly, it has been suggested that sound barriers, erected to reduce noise, may prove effective at decreasing pollutant concentrations (Steffens *et al.*, 2013). In spite of the accumulating evidence, uncertainties regarding the effects of roadside noise barriers on pollutant concentrations in surrounding areas remain. Although there are much CFD studies about pollution dispersion around noise barrier (Jeong, 2014, 2013; Steffens *et al.*, 2013; Jeong 2012a, b; Hagler *et al.*, 2011), the role of road configuration plus noise barrier has not been fully investigated.

The dispersion of air pollutions in complex situations such as the case of noise barriers in close proximity is a difficult problem, but important for the safety of people living and working in such areas. Computational fluid dynamics (CFD) provides a method to build and run models that can simulate air pollution in such geometrically complex situations; however, the accuracy of the results needs to be assessed (Finn *et al.*, 2010).

In this study, we utilized the CFD model to simulate the pollution dispersion around various road configuration plus noise barrier. The goals of the study were (1) to investigate the effects of a roadway barrier and road configuration on air pollution dispersion around road and (2) to suggest the horizontal and vertical impact distances of roadway emissions.

2. MATERIALS AND METHODS

2.1 Numerical Method

FLUENT CFD software (FLUENT, 2006) was used

to simulate wind flow and pollutant concentration around road and noise barriers. The Reynolds-averaged Navier-Stokes (RANS) equations were used to simulate the processes of interest. Mass and momentum conservation equation are written as follows,

$$\frac{\partial \rho}{\partial t}+\frac{\partial}{\partial x_i}(\rho u_i)=0 \tag{1}$$

$$\frac{\partial}{\partial t}(\rho u_i)+\frac{\partial}{\partial x_j}(\rho u_i u_j) = -\frac{\partial p}{\partial x_i}+\frac{\partial}{\partial x_j}\left[\mu\left(\frac{\partial u_i}{\partial x_j}+\frac{\partial u_j}{\partial x_i}-\frac{2}{3}\delta_{ij}\frac{\partial u_l}{\partial x_l}\right)\right] + \frac{\partial}{\partial x_j}\left(-\rho\overline{u_i' u_j'}\right) \tag{2}$$

Where u_j is the j component of velocity, t is the time, x_j is the j coordinate, ρ is the air density, μ is the dynamic viscosity;

$$-\rho\overline{u_i' u_j'}=\mu_t\left(\frac{\partial u_i}{\partial x_j}+\frac{\partial u_j}{\partial x_i}\right)-\frac{2}{3}\left(\rho k+\mu_t\frac{\partial u_k}{\partial x_k}\right)\delta_{ij} \tag{3}$$

is the Reynolds stress; $\mu_t=\rho C_\mu\frac{k^2}{\varepsilon}$ is the turbulent viscosity.

Among the standard, RNG and realizable $k-\varepsilon$ turbulence model, realizable $k-\varepsilon$ turbulence model provides the most consistent agreement for both the 1H (where H is barrier height) barrier and no-barrier models (Hagler *et al.*, 2011). So, the realizable $k-\varepsilon$ model was utilized for all simulations in this study. The governing equations of realizable $k-\varepsilon$ turbulence model are

$$\frac{\partial}{\partial t}(\rho k)+\frac{\partial}{\partial x_j}(\rho k u_j)=\frac{\partial}{\partial x_j}\left[\left(\mu+\frac{\mu_t}{\sigma_k}\right)\frac{\partial k}{\partial x_j}\right] +G_k+G_b-\rho\varepsilon-Y_M+S_k \tag{4}$$

$$\frac{\partial}{\partial t}(\rho \varepsilon)+\frac{\partial}{\partial x_j}(\rho \varepsilon u_j)=\frac{\partial}{\partial x_j}\left[\left(\mu+\frac{\mu_t}{\sigma_\varepsilon}\right)\frac{\partial \varepsilon}{\partial x_j}\right] +\rho C_1 S\varepsilon-\rho C_2\frac{\varepsilon^2}{k+\sqrt{v\varepsilon}}+C_{1\varepsilon}\frac{\varepsilon}{k}C_{3\varepsilon}G_b+S_\varepsilon \tag{5}$$

Where $C_1=\max\left[0.43, \frac{\eta}{\eta+5}\right]$, $\eta=S\frac{k}{\varepsilon}$, $S=\sqrt{2S_{ij}S_{ij}}$, $S_{ij}=\frac{1}{2}\left(\frac{\partial u_j}{\partial x_i}+\frac{\partial u_i}{\partial x_j}\right)$.

In these equations, G_k represents the generation of turbulence kinetic energy due to the mean velocity gradients, G_b is the generation of turbulence kinetic energy due to buoyancy, Y_M represents the contribution of the fluctuating dilatation in compressible tur-

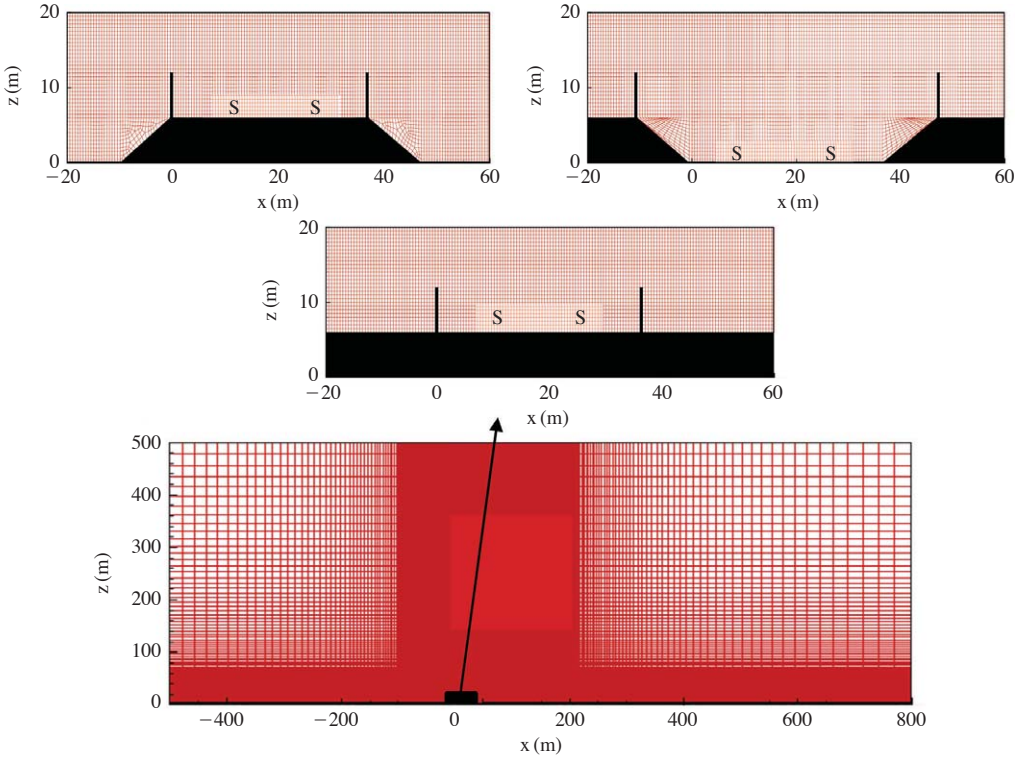

Fig. 1. Schematic diagram of computational domain and barrier position for three road configurations (S is source).

bulence to the overall dissipation rate. σ_k (=1.0) and σ_ε (=1.2) are turbulent Prandtl numbers for k and ε, respectively.

For all simulations, RANS equations (1), (2), and two turbulence closure equations (4), (5) for realizable $k-\varepsilon$ for the turbulent kinetic energy (k) and for the dissipation rate of turbulent kinetic energy (ε) equations are solved in each case, respectively.

The pollutant dispersion patterns were analyzed after solving the species transport equation in conjunction with the turbulence model equations. The advection–diffusion (AD) module was applied to study the species transport process by analyzing the mass fraction of pollutants in the mixture. FLUENT analyzes the mass diffusion process based on the following equations (Ng and Chaw, 2014; Riddle *et al*., 2004):

$$J_i = -\left(\rho D + \frac{\mu_t}{Sc_t}\right)\nabla y \tag{6}$$

where J_i is the diffusion flux of the mixture (kg/m^{2}s), ρ is the density of the mixture (kg/m^3), D is the mass diffusion coefficient of the pollutant in the mixture (m^2/s), y is the mass fraction of the pollutant (kg/kg), μ_t is the turbulent viscosity (kg · s/m). Turbulent Schmidt number Sc_t was specified 0.7 in this study.

2.2 Computational Domain and Boundary Conditions

Fig. 1 shows three types of road shape, noise barrier and the computational domain of this study. With re-

Table 1. Inlet and boundary conditions in this study.

Boundary conditions	Type	Remarks
Bottom	Wall	No slip condition Roughness height=0.24 m, Roughness constant=1.428
Inlet	Velocity-inlet	Velocity Magnitude=UDF[a], TKE[b]=UDF, TDR[c]=UDF Friction velocity=0.512 m/s, z_0=0.035 m
Outlet	Pressure-outlet	Backflow TKE=0 and TDR=0
Top	Symmetry	Top
Source	Mass-flow-inlet	Mass flow-rate=0.01 kg/s, TKE=0, TDR=0 CO Species mass fraction=1.0
Noise barrier	Wall	No slip condition Roughness height=0.24 m, Roughness constant=1.428

[a]UDF=User Defined Function
[b]TKE=Turbulent Kinetic Energy
[c]TDR=Turbulent Dissipation Rate

Table 2. Simulation case of various road plus barrier types in this study.

Cases	Road shape	Barrier position	Barrier number	Road configuration
A-I	At-grade	None	0	
A-II	At-grade	Windward	1	
A-III	At-grade	Leeward	1	
A-IV	At-grade	Windward & Leeward	2	
F-I	Filled	None	0	
F-II	Filled	Windward	1	
F-III	Filled	Leeward	1	
F-IV	Filled	Windward & Leeward	2	
D-I	Depressed	None	0	
D-II	Depressed	Windward	1	
D-III	Depressed	Leeward	1	
D-IV	Depressed	Windward & Leeward	2	

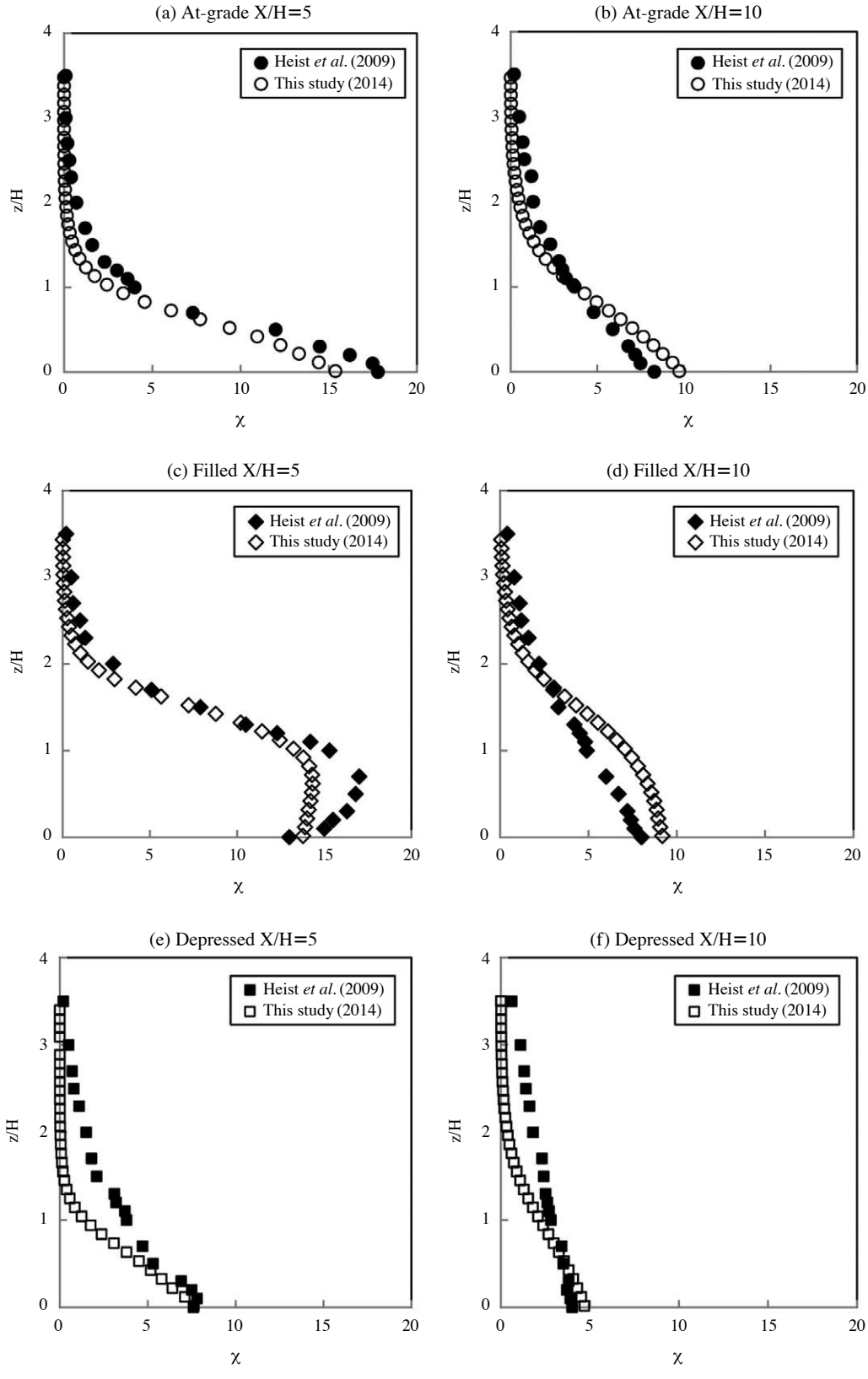

Fig. 2. Comparison of concentration profiles between model and wind tunnel results.

gard to the grid design, Bourdin and Wilson (2008) suggested that the upstream (inlet) and downstream (outflow) boundaries should be located at least 20 barrier heights away from the noise barrier, the top boundary should be at least 40 barrier heights above the noise barrier. In this study, inlet and outlet boundaries are located at −500 m, and 800 m respectively and top boundary is 500 m height. Because barrier height was 6 m in this study, the boundary conditions of Bourdin and Wilson (2008) are satisfied. The atmospheric stability condition was neutral and road emission source height was located at z=0 m in this study.

According to the other CFD modeling studies (Yang *et al*., 2009; Gorle *et al*., 2009; Richards and Hoxey, 1993), the horizontal inhomogeneity of the wind flow profiles can result in unanticipated errors which can be particularly significant for pedestrian-level wind conditions. Richards and Hoxey (1993) suggested inflow boundary conditions of mean wind speed and turbulence quantities for the standard $k-\varepsilon$ model that satisfied the transport equations for k and ε.

Yang *et al*. (2009) derived the solution of the k equation of the standard $k-\varepsilon$ model and proposed a new set of inflow turbulence boundary conditions. Inlet boundary condition for U in the neutral boundary condition is;

$$U(z)=\frac{u_*}{k}\ln\left(\frac{z+z_0}{z_0}\right) \tag{7}$$

Where u_* is friction velocity; k is von Karman constant; z_0 is roughness length and z is height from surface. According to Gorle *et al*. (2009), if equilibrium between turbulence dissipation and production is imposed, the profile for k and ε have following form.

$$k(z)=\sqrt{A\ln(z+z_0)+B} \tag{8}$$

Where A and B are constants that can be determined by fitting the equations to the measured profiles of k. Using turbulent kinetic energy profile for neutral condition of Lin *et al*. (2009) the profile under consideration $A=-0.075$ and $B=0.478$ were selected in this study. The profile of ε is given by;

$$\varepsilon(z)=\frac{\sqrt{C_\mu}u_*}{k(z+z_0)}\sqrt{A\ln(z+z_0)+B} \tag{9}$$

When using a commercial CFD code, however, the wall boundary condition is usually not as prescribed above. Blocken *et al*. (2007) provide a solution for this by deriving a relationship which brings the rough wall functions in equilibrium with the inlet profiles. For FLUENT this relation is given by:

$$k_s=\frac{9.793z_0}{C_s} \tag{10}$$

Where k_s is the roughness height and C_s is a constant required for the wall function. Roughness height should be smaller than the height of the center point of the wall adjacent cell and was consequently set to 0.24 m in this study. The resulting value for C_s is 1.428 is defined through a User Defined Function. Table 1 listed boundary conditions used in this study.

The baseline case was the reference case with no barriers (Heist *et al*., 2009). This was a 1 : 150 scale wind tunnel model corresponding to the full-scale equivalent value of barrier height H is 6 m. In order to investigate the effects of road configuration plus noise barrier on air pollution dispersion around the road, 12 simulation cases were selected in this study. As shown in Table 2, these were 4 of at-grade (Cases of A-I ~ A-IV), 4 of filled (Cases of F-I ~ F-IV), and 4 of depressed cases (Cases of D-I ~ D-IV). Noise barriers were positioned

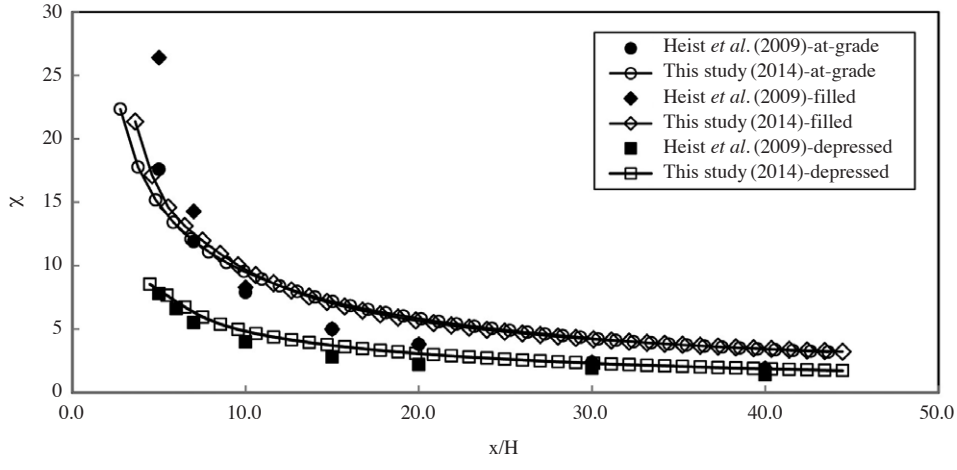

Fig. 3. Comparison of surface concentrations between model and wind tunnel results.

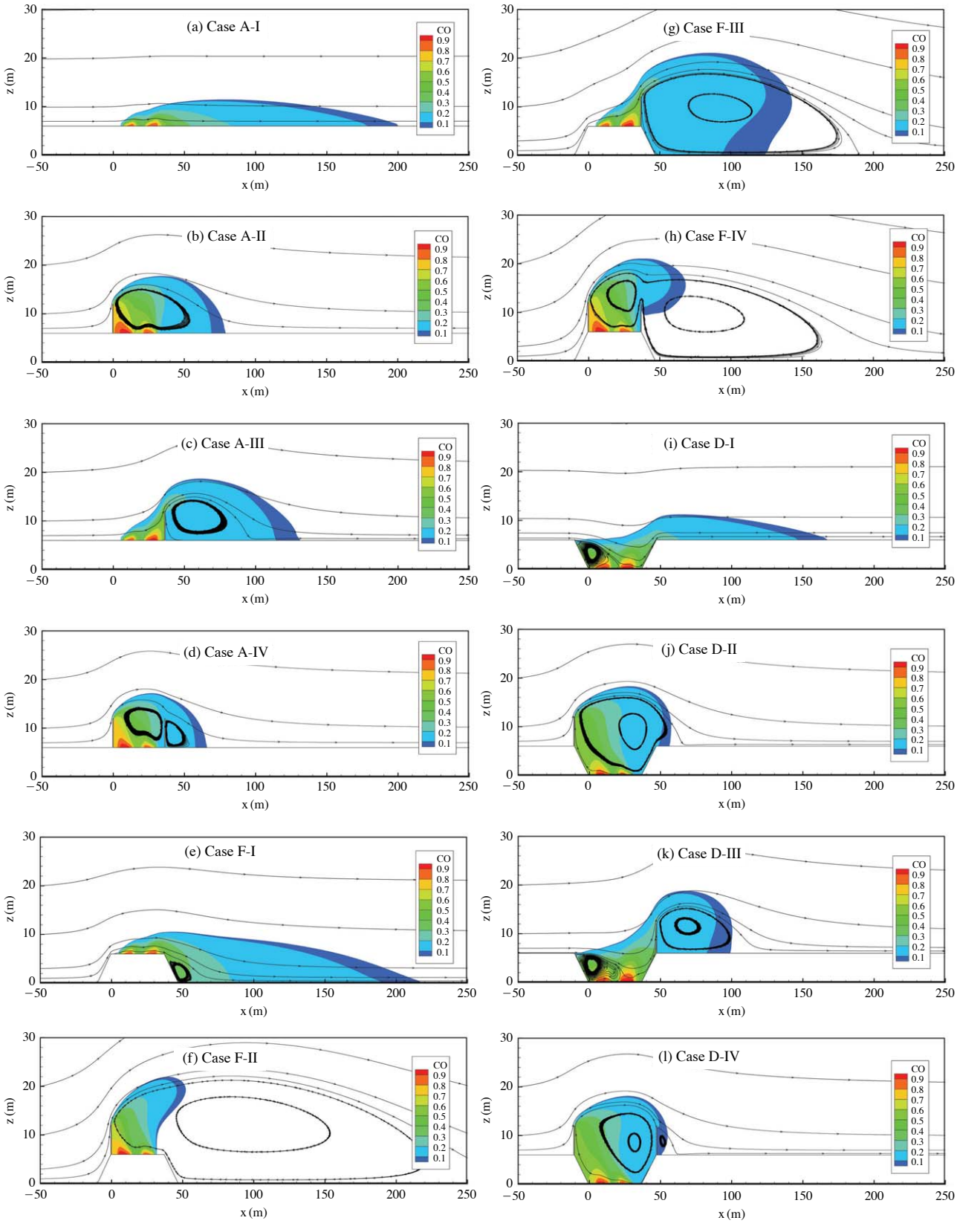

Fig. 4. Concentration contours and streamlines for various simulation cases.

none, windward, leeward, and wind and leeward, respectively.

3. RESULTS AND DISCUSSION

3.1 Evaluation of CFD Model with Wind Tunnel Experimental Data

To evaluate the performance of FLUENT model the Figs. 2 to 3 show selected concentration profiles of the simulation and experiment results. In these figures data for Heist *et al*. (2009) is wind tunnel results of neutral stability condition.

In this study, we selected carbon monoxide as the target material. The concentrations were normalized to give the non-dimensional concentration $X=CU_rL_xL_y/Q$ (Heist *et al*. (2009), where C is the concentration (a fraction by mass), U_r is the reference wind speed (equal to 12 m/s, calculated at a full-scale equivalent height of 500 m), Q is the mass flow rate (0.01 kg/s of carbon monoxide), L_x is the length of the line source (30 m), and L_y is the lateral length of the source segment (Because simulation was conducted 2-dimensional domain in this study, L_y=1 m was used). The length scale (X/H) was normalized with height of barrier (H=6 m).

Fig. 2 shows concentration profile of no barrier cases for three road cases at X/H=5 and 10 positions. The overall modeling results show similar tendency with experimental results but modeling results of surface concentrations at X/H=5 (Fig. 2(a), (c)) are about 20% smaller than that of wind tunnel result. Modeling result of surface concentration at X/H=10 (Fig. 2(f)) is about 25% larger than that of wind tunnel result.

Fig. 3 shows the comparison between calculated and experimental results of normalized surface concentrations at z=1 m height. There is good agreement between experimental data and CFD simulated results for a similar configuration. At a distance from source to the X/H=6.0, however, modeling results of at-grade and filled case have 1.5-2.0 times smaller than that of experimental results.

3.2 Effect of Road Shape and Noise Barrier on Dispersion of Road Emission

Fig. 4 shows streamline and concentration of 12 simulated cases. As shown in Fig. 4, streamlines show various flow patterns around road configurations and the low concentration region has been attributed to upward deflection of the airflow and increased vertical mixing due to the barrier. These figures are used to

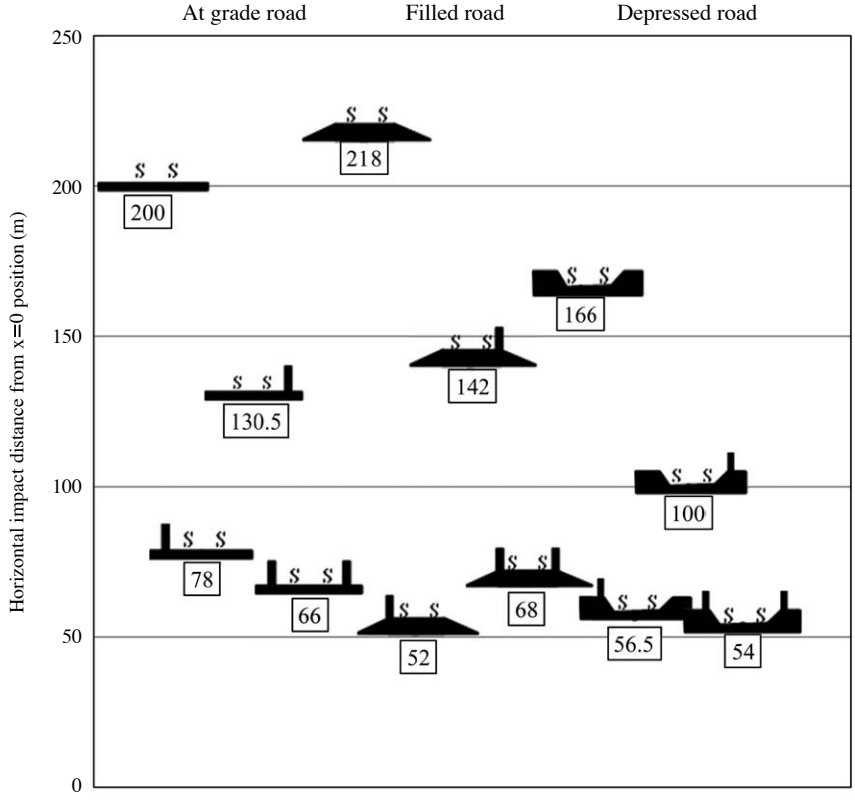

Fig. 5. Comparison of horizontal impact distance of various road configurations plus barrier types (Numbers in boxes are horizontal impact distances from x=0).

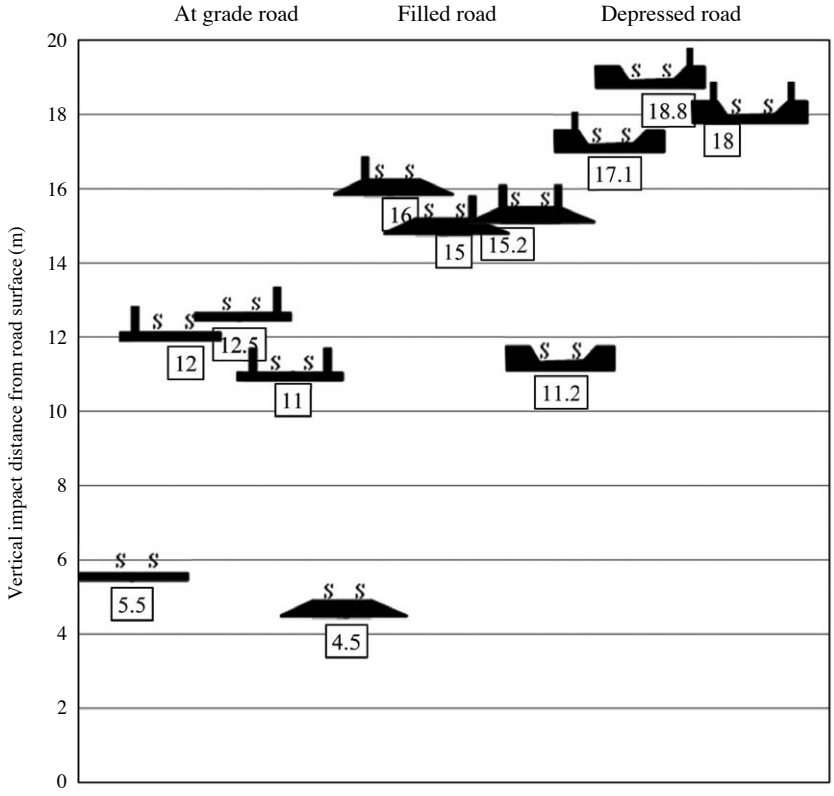

Fig. 6. Comparison of vertical impact distance of various road configurations and barrier types (Numbers in boxes are vertical impact distances from road surface).

evaluate the impact distance of road shape and barriers on the dispersion of road air pollutants.

To compare the horizontal and vertical impact distance of road shape plus noise barrier on road emission of simulated cases, Figs. 5-6 represented 12 simulated cases. It should be noted, that the proposed impact distance was concentration of mass fraction larger than 0.1 was used. The largest horizontal impact distance was 218 m (case F-I) and the smallest horizontal impact distance was 52 m (case F-II) in Fig. 6. Depressed road shows short horizontal impact distance. This means retention of vehicle emission in depressed road is larger than that of at-grade and filled road. The largest vertical impact distance was 18.8 m (case D-III) and the smallest vertical impact distance was 4.5 m (case F-I).

4. CONCLUSIONS

The dispersion of vehicle emission forming various road shape plus barrier were evaluated using FLUENT CFD model. Simulated road shapes are three types, namely at-grade, depressed, and filled road. The realizable $k-\varepsilon$ model in FLUENT CFD code was used to simulate the flow and dispersion around road. The selected concentration profile results were compared with the wind tunnel experiments. The overall simulated results agree well wind the wind tunnel experimental results. Generally, filled road had the largest horizontal impact distance (larger 3.33~3.55 times than those of no barrier case) and depressed road had the largest vertical impact distance (1.53~1.68 times compare with no barrier case).

REFERENCES

Blocken, B., Stathopoulos, T., Carmeliet, J. (2007) CFD simulation of the atmospheric boundary layer: wall function problems. Atmospheric Environment 41, 238-252.

Bourdin, P., Wilson, J.D. (2008) Windbreak Aerodynamics: Is Computational Fluid Dynamics Reliable? Boundary-Layer Meteorology 126, 181-208.

Finn, D., Clawson, K.L., Carter, R.G., Rich, J.D., Eckman, R.M., Perry, S.G., Isakov, V., Heist, D.K. (2010) Tracer studies to characterize the effects of roadside noise barriers on near-road pollutant dispersion under varying atmospheric stability conditions. Atmospheric Envi-

ronment 44, 204-214.
FLUENT ver.6.3 (2006) User's Guide.
Gorle, C., Beeck, J., Rambaud, P., Tendeloo, G.V. (2009) CFD modelling of small particle dispersion: The influence of the turbulence kinetic energy in the atmospheric boundary layer. Atmospheric Environment 43, 673-681.
Hagler, G.S.W., Tang, W., Freeman, M.J., Heist, D.K., Perry, S.G., Vette, A.F. (2011) Model evaluation of roadside barrier impact on near-road air pollution. Atmospheric Environment 45, 2522-2530.
HEI (2010) Traffic-related air pollution: a critical review of the literature on emissions, exposure, and health effects. HEI special report 17. Boston, MA: Health Effects Institute.
Heist, D.K., Perry, S.G., Brixey, L.A. (2009) A wind tunnel study of the effect of roadway configurations on the dispersion of traffic-related pollution. Atmospheric Environment 43, 5101-5111.
Jeong, S.J. (2012a) A study on Air Pollution Dispersion around Multi-noiseBarrier (II)- Double noise. Korean Journal of Odor Research And Engineering 11(3), 119-125. (in Korean)
Jeong, S.J. (2012b) A study on Air Pollution Dispersion around a Filled Road. Journal of Korean Society of Odor Research And Engineering 11(4), 184-190. (in Korean)
Jeong, S.J. (2013) A study on air pollution dispersion around a depressed road using CFD modeling. Journal of Korean Society of Odor Research And Engineering 12(2), 43-50. (in Korean)
Jeong, S.J. (2014) Effect of Double Noise-Barrier on Air Pollution Dispersion around Road, Using CFD. Asian Journal of Atmospheric Environment 8(2), 81-88.
Lin, X.J., Barrington, S., Choiniere, D., Prasher, S. (2009) Effect of weather conditions on windbreak odour dispersion. Journal of Wind Engineering and Industrial Aerodynamics 97, 487-496.
Ng, W.Y., Chau, C.K. (2014) A modeling investigation of the impact of street and building configurations on personal air pollutant exposure in isolated deep urban canyons. Science of the Total Environment, 468-469, 429-448.
Richards, P.J., Hoxey, R.P. (1993) Appropriate boundary conditions for computational wind engineering models using the k-e model. Journal of Wind Engineering and Industrial Aerodynamics 46 & 47, 145-153.
Riddle, A., Carruthers, D., Sharpe, A., Stocker, C.M.J. (2004) Comparisons between FLUENT and ADMS for atmospheric dispersion modeling. Atmospheric Environment 38, 1029-1038.
Steffens, J.T., Heist, D.K., Perry, S.G., Zhang, K.M. (2013) Modeling the effects of a solid barrier on pollutant dispersion under various atmospheric stability conditions. Atmospheric Environment 69, 76-85.
Yang, Y., Gu, M., Chen, S., Jin, X. (2009) New inflow boundary conditions for modelling the neutral equilibrium atmospheric boundary layer in computational wind engineering. Journal of Wind Engineering and Industrial Aerodynamics 97(2), 88-95.

(Received 20 August 2014, revised 26 January 2015, accepted 6 February 2015)